Nanoporous Materials

DOI: 10.1002/anie.201208501

Bottom-Up Synthesis of Monodispersed Single-Crystalline Cyano-Bridged Coordination Polymer Nanoflakes

Ming Hu, Shinsuke Ishihara, and Yusuke Yamauchi**

Coordination polymers (CPs), including metal–organic frameworks (MOFs), porous coordination polymers (PCPs), and Prussian blue analogues, have received attention in recent years because their adjustable pore structures and their framework compositions make them attractive materials for many applications.[1] Currently, the nanostructural control of CPs has become increasingly interesting due to their unique size- and shape-dependent properties, which differ from those of bulk crystals.[2–4]

On the other hand, a two-dimensional (2D) morphology is interesting because it shows many properties that are not observable in bulk chemistry.[5] For example, in graphite, various unique properties, such as the electric field effect, quantum Hall effect, and superthermal conductivity, can be observed on monolayer graphene nanosheets.[5a,b] For electrochemical applications, enhanced cycling stability, larger discharge capacity, and efficient lithium insertion can be realized on 2D nanosheets/nanofilms/nanoflakes.[5c–f] Similar effects can be expected in 2D CP nanosheets/nanofilms/nanoflakes. The 2D CPs can offer a highly accessible surface area that permits guest molecules to effectively enter the micropores in the CPs. Moreover, 2D CPs can provide many active sites for catalytic and electrochemical reactions, and furthermore assembled CPs can be used as membrane filters.

Several efforts have thus been made towards the successful preparation of 2D CPs.[6] Kitagawa et al. prepared an MOF-2 nanofilm using a layer-by-layer growth method.[6a] Xu et al.[6b] proposed a top-down delamination process from bulk crystals of a layered MOF, and Cheetham et al.[6c] reported ultrasonication-induced exfoliation approach to prepare MOF nanosheets. Although some important advantages have been identified in previous research, we believe that the approaches are somewhat inconvenient because of the need for complicated synthetic conditions and special equipment. Therefore, developing a facile and large-scale preparation method can allow further extensive research toward practically useful 2D CPs.

Herein, we report novel bottom-up synthesis of monodispersed 2D CP nanoflakes through an aqueous solution approach. Our target CP, $Ni(H_2O)_2[Ni(CN)_4]\cdot x\,H_2O$, is known as a layered Hofmann-type CP in which the neighboring Ni atoms are bridged by the cyano group.[7] For the preparation of cyano-bridged CP nanoflakes, $NiCl_2\cdot 6\,H_2O$ and trisodium citrate dihydrate were dissolved in pure water to form a clear solution. Meanwhile, $K_2[Ni(CN)_4]$ was added into pure water to form another clear solution. The two solutions were then mixed and aged at room temperature for 24 h. The experimental details are given in the Supporting Information. Hereafter, the product is defined as "Ni-CP." A colloidal suspension of well-dispersed Ni-CP nanoflakes is shown in Figure 1 a-1. A clear Tyndall light-scattering effect was observed by a side-incident light beam. A TEM image of the Ni-CP nanoflakes is shown in Figure 1 a-2. A TEM grid was immersed in the colloidal suspension for one minute, and this was followed by rinsing with a copious amount of water and drying under a N_2 stream. The nanoflakes with a submicrometer lateral size were routinely observed. According to the selected-area electron diffraction (ED) patterns (inset of Figure 1 a-2), each nanoflake has a single-crystalline nature. A high-resolution TEM image of the edge part of the nanoflake also showed that all the lattice fringes were oriented in the same direction without any domain boundary (Figure 1 a-3).

The synthesized Ni-PC nanoflakes were collected and washed several times with pure water and ethanol. The crystal structure of the obtained Ni-CP was confirmed by wide-angle XRD measurements (Supporting Information, Figure S1). All of the diffraction peaks could be assigned as an orthorhombic system, which matched the Hofmann-type $Ni(H_2O)_2[Ni(CN)_4]\cdot x\,H_2O$ CP with a 2D layered structure.[7] No impurity phases were observed. From elemental analysis, it was confirmed that the composition was $Ni(H_2O)_2[Ni(CN)_4]\cdot 3\,H_2O$. As seen in Figure 1 b, all the products show the typical 2D flake morphology. Many nanoflakes were randomly aggregated over the entire area. From a cross-sectional SEM image, the thicknesses of the nanoflakes ranged from 5 nm to 10 nm, while the lateral sizes were larger than 100 nm. Considering that a single layer of Ni-CP should be 0.7 nm in thickness (Figure 1 c), our obtained nanoflakes

[*] Dr. M. Hu, Dr. S. Ishihara
International Center for Young Scientists (ICYS)
National Institute for Materials Science (NIMS)
1-1 Namiki, Tsukuba, Ibaraki 305-0044 (Japan)
Dr. M. Hu, Dr. S. Ishihara, Prof. Dr. Y. Yamauchi
World Premier International (WPI) Research Center for Materials Nanoarchitectonics (MANA)
National Institute for Materials Science (NIMS)
1-1 Namiki, Tsukuba, Ibaraki 305-0044 (Japan)
E-mail: hu.ming@nims.go.jp
yamauchi.yusuke@nims.go.jp
Homepage: http://www.yamauchi-labo.com
Prof. Dr. Y. Yamauchi
Faculty of Science and Engineering, Waseda University
3-4-1 Okubo, Shinjuku, Tokyo 169-8555 (Japan)
Prof. Dr. Y. Yamauchi
Precursory Research for Embryonic Science and Technology (PRESTO) (Japan) Science and Technology Agency (JST)
4-1-8 Honcho, Kawaguchi, Saitama 332-0012 (Japan)

Supporting information for this article is available on the WWW under http://dx.doi.org/10.1002/anie.201208501.

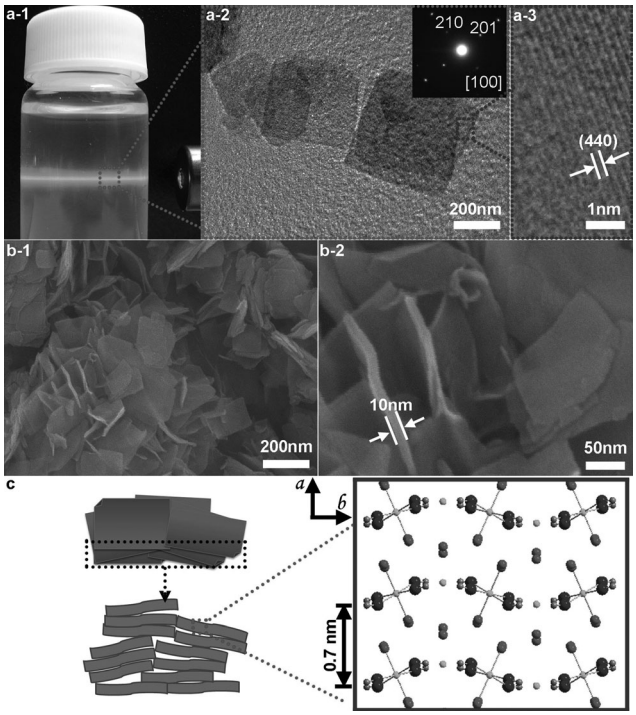

Figure 1. a-1) Photographs of colloidal suspensions containing well-dispersed 2D CP nanoflakes. The light beam is incident from the side to demonstrate the Tyndall effect. a-2) Low-magnified TEM image of the obtained nanoflakes. Inset: corresponding selected-area electron diffraction (ED) pattern taken from a single nanoflake. a-3) A high-resolution TEM image taken from the edge of a single nanoflake. b) SEM images of the nanoflakes. c) Illustration of assembled CP nanoflakes after solvent evaporation and their crystal structure.

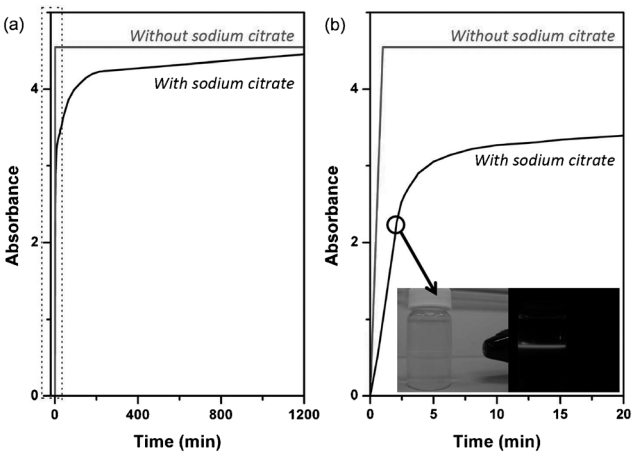

Figure 2. a) Time-dependent absorbance change measured from the UV/Vis absorption at 421 nm during the Ni-CP crystallization process in the presence and absence of trisodium citrate. b) Time-dependent absorbance at the early stage (0–20 min). Inset: the solution at the early stage of the Ni-CP crystallization process. The light beam is incident from the side to demonstration the Tyndall effect.

appeared to be composed of several stacked layers (that is, multiple layers).

To understand the formation mechanism of Ni-CP nanoflakes, a control experiment was performed. Without the addition of trisodium citrate, the reaction was terminated very rapidly within 1 min, and only irregular nanoparticles with polycrystalline nature were obtained (Supporting Information, Figure S2). Obviously, trisodium citrate is a crucial factor for the generation of 2D Ni-CP nanoflakes. From the UV/Vis spectra (Supporting Information, Figure S3), it is evident that, after the addition of trisodium citrate, the strength of the maxima absorption peak of $NiCl_2$ solution was significantly increased and the position was shifted. This absorbance variation was caused by coordination between citrate ions and Ni^{2+} ions.[8] This chelating effectively prevented the rapid coordination reaction between Ni^{2+} and $[Ni(CN)_4]^{2-}$ (as a ligand), resulting in the deceleration of the crystallization process of Ni-CP. To further confirm this effect, the solutions at different reaction times were characterized by real-time UV/Vis measurement (Figure 2). In the presence of trisodium citrate, the absorbance at 421 nm (indicating the formation of Ni-CP) increased very slowly. In contrast, in the absence of trisodium citrate, very fast formation of Ni-CP was confirmed, and the reaction was terminated within 1 min. Thus, by the addition of trisodium citrate, the Ni-CP crystallization process was extended to 20 h.

To illustrate the role of citrate ions more clearly, we performed a ^1H NMR study. ^1H NMR study more clearly revealed the chelating effect of the sodium citrate with Ni^{2+} ions. As shown in the Supporting Information, Figure S4 a-b, the ^1H NMR spectra of the citrate ligand appearing as two doublet peaks at around 2.6 ppm disappeared in the presence of $NiCl_2$, which is typical in the formation of a metal–ligand complex involving paramagnetic ions.[9] This phenomenon supports our observation from the UV/Vis data. After the addition of the $K_2[Ni(CN)_4]$ solution in the mixed solution of sodium citrate and $NiCl_2$, the ^1H NMR peak at around 2.6 ppm gradually recovered (Supporting Information, Figure S4 c-i), and was accompanied by the visible precipitation of white solids. This result indicates that citrate anions are becoming free from paramagnetic Ni^{2+}. The free Ni^{2+} ions released from the citrate complex could gradually react with $K_2[Ni(CN)]_4$ to generate Ni-CP. Thus, the ^1H NMR study revealed that citrate anions can work to stabilize the Ni^{2+} ions in the solution, which delay the generation speed of Ni-CP drastically.

In general, rapid crystallization generally results in fine nanoparticles with irregular shapes, while very slow crystallization can allow growing crystals to develop a well-defined macroscopic morphology similar to the inherent atomic crystal structure. In our case, Ni-CPs show a flake-like morphology, which corresponds to the layered crystal structure (Figure 1 c). To further demonstrate this concept is general, trisodium citrate was utilized to other CPs with layered structures. Two Hoffman-type CPs, $Co(H_2O)_2[Ni(CN)_4]\cdot 3H_2O$[7a] and $Cu(H_2O)_2[Pt(CN)_4]\cdot 2H_2O$[7d] were selected as examples (Supporting Information, Figure S5). Without using sodium citrate, irregularly-shaped nanoparticles were obtained. When appropriate amount of sodium citrate were used, unifom nanoflakes were obtained.

It is well-known that Hofmann-type Ni-CPs exhibit nanoporosity after removing the coordinated water molecules

at the interlayer space.[7a] The adsorption–desorption isotherm of the obtained Ni-CP nanoflakes showed a significant increase at low P/P_0 (Supporting Information, Figure S6a), which corresponds to the presence of micropores with a pore size less than 2 nm (Supporting Information, Figure S6b). The BET surface area of the Ni-CP nanoflakes was calculated to be 150 $m^2 g^{-1}$ (Supporting Information, Figure S6a). The high porosity was attributed to the random assembly of the layered nanoflakes, as illustrated in Figure 1c. According to the Horvath and Kawazoe (HK) method (Supporting Information, Figure S6b), the pore size distribution was too different from that of other microporous materials, such as zeolites. In contrast, the Ni-CP nanoparticles prepared without trisodium citrate had a much lower surface area of 47 $m^2 g^{-1}$. Irregularly shaped particles were densely packed after degassing, resulting in an undeveloped porous structure with a very low surface area.

A promising utilization of CPs is the conversion into nanostructured metal oxide and carbon materials.[10,11] Owing to their inorganic–organic hybrids, CPs are considered as excellent precursors for nanoporous inorganic materials.[10,11] Considering cyano-bridged CPs, the percentages of metal components are generally high. Therefore, by removing the C–N part by thermal treatment, we can convert 2D CP nanoflakes into flake-shaped nanoporous metal oxides. Here, we demonstrated that the obtained Ni-CP nanoflakes were successfully converted into nanoporous nickel oxide (NiO). In general, NiO/Ni is one of the most important materials owing to its wide applicability in many research fields. Among these applications, its use as an electrochemical pseudocapacitor material is interesting[12] because of the social requirements for energy storage materials. Nanoporous NiO/Ni electrodes with high surface areas and unique shapes are promising candidates for high-capacitance energy storage.

The synthesized Ni-CP nanoflakes were calcined at different temperatures to prepare various nanoporous NiO/Ni samples with different crystal phases and sizes. Wide-angle XRD patterns for various samples are shown in the Supporting Information, Figure S7. Only the sample obtained at 300 °C was pure nickel oxide, while the other two samples obtained at 400 °C and 500 °C were mixed phases of both Ni and NiO. The reason for the generation of Ni at higher temperature may be that the thermal decomposition of Ni-CPs at high temperature is much faster than that at low temperature. Therefore, the breaking off of C–N units between two Ni atoms is faster than the formation of Ni–O bonds, thereby forming the un-oxidized Ni phase in some parts.

Figure 3 shows SEM and TEM images of the samples calcined at 300 °C, 400 °C, and 500 °C. The sample calcined at 300 °C preserved flake-like morphology (Figure 3a-1). A TEM image and the corresponding ED patterns confirmed that the nanoflakes were well-crystallized into the NiO phase (Figure 3a-2). On the other hand, as the applied temperatures gradually increased, the original flake-like morphology was lost because a serious thermal fusion occurred (Figure 3b,c). The specific surface areas of the obtained samples were examined by N_2 gas adsorption–desorption isotherms. For the sample calcined at 300 °C, a highly porous structure was

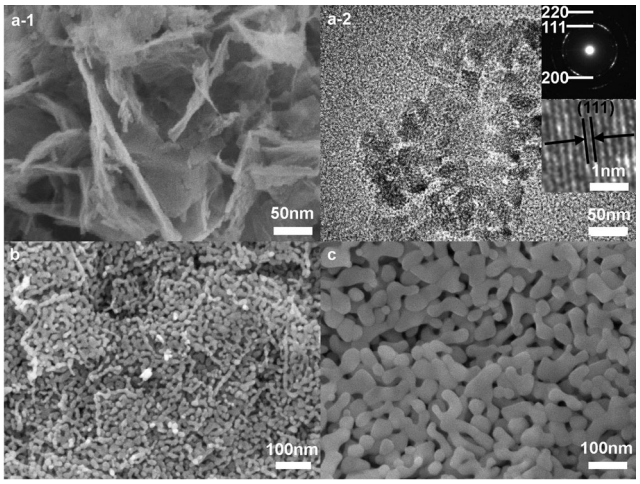

Figure 3. a-1) SEM and a-2) TEM images of NiO sample obtained by calcination at 300 °C. Inset images: the corresponding selected-area ED patterns taken from a single nanoflake and a high-resolution TEM image of the edge of the nanoflake. b) SEM image of NiO/Ni sample obtained by calcination at 400 °C. c) SEM image of NiO/Ni sample obtained by calcination at 500 °C.

successfully realized. The significant increase at low P/P_0 indicated the existence of micropores, while the steady increase from 0.1 to 0.5 of P/P_0 indicated the formation of widely distributed mesopores that were created by the aggregated form of the flakes (Supporting Information, Figure S8). Because of such hierarchically porous architecture, the surface area reached 240 $m^2 g^{-1}$, which is a high value in comparison with that obtained with mesoporous NiO[13] and commercially available NiO powders. In contrast, for two other samples at higher temperatures, the surface areas were drastically decreased because the nanoporous structures collapsed as a result of the progress of the crystallization.

Highly crystalline NiO with a high surface area (calcined at 300 °C) is useful as a pseudocapacitor material. The rate-dependent cyclic voltammetry curve is given in the Supporting Information, Figure S9a. Two strong current peaks correspond to a redox reaction ($NiO + OH^- \leftrightarrow NiO(OH) + e^-$). Such typical behavior mainly resulted from a pseudocapacitance based on a fast redox mechanism. As shown in the Supporting Information, Figure S9b, the specific capacitance obtained at a scanning rate at 5 $mV s^{-1}$ was around 365 $F g^{-1}$, which was much higher than those of other samples (NiO/Ni samples obtained at 400 °C and 500 °C and commercially available NiO powders). This was because the high surface area of nanoporous NiO offered more places for a redox reaction between the electrolyte and the NiO phase.

We also observed a decrease of the capacitance at a higher scanning rate (at 25 $mV s^{-1}$; Supporting Information, Figure S9b). For two samples calcined at 400 °C and 500 °C, large capacitance losses (60–80 %) were observed. This decrease is due to barriers to penetration and diffusion of electrolytes (that is, some parts of the electrode surface become inaccessible at high charging–discharging rates). This is common for other electrochemical supercapacitors.[14] However, for nanoporous NiO calcined at 300 °C, only 30 % of the capacitance

loss was found, which resulted from the effective mass transportation through the hierarchical porous structure developed by the nanoflake assembly. Furthermore, the nanoporous NiO showed excellent cycle stability, which is required for practical applications. The capacitance retention increased slightly to 5% after the first 200 cycles instead of decreasing, as in most cycling stability tests reported elsewhere.[15] The capacitance loss after 2000 cycles was only 10%.

In conclusion, we have proposed a novel solution synthesis to prepare 2D Ni-CP nanoflakes with a controlled crystallization process. We strongly believe that our bottom-up approach will be useful for preparation of other types of CPs nanoflakes. Such 2D shaped-CPs and their derivatives will give us great opportunity for new solid state properties in future.

Received: October 22, 2012
Published online: December 3, 2012

Keywords: coordination polymers · cyano bridges · nanoporous materials · nickel oxide

[1] a) O. M. Yaghi, M. O'Keeffe, N. W. Ockwig, H. K. Chae, M. Eddaoudi, J. Kim, *Nature* **2003**, *423*, 705; b) S. Kitagawa, R. Kitaura, S. Noro, *Angew. Chem.* **2004**, *116*, 2388; *Angew. Chem. Int. Ed.* **2004**, *43*, 2334; c) X. B. Zhao, B. Xiao, A. J. Fletcher, K. M. Thomas, D. Bradshaw, M. J. Rosseinsky, *Science* **2004**, *306*, 1012; d) O. K. Farha, A. Ö. Yazaydın, I. Eryazici, C. D. Malliakas, B. G. Hauser, M. G. Kanatzidis, S. T. Nguyen, R. Q. Snurr, J. T. Hupp, *Nat. Chem.* **2010**, *2*, 944; e) S. T. Meek, J. A. Greathouse, M. D. Allendorf, *Adv. Mater.* **2011**, *23*, 249; f) M. C. Das, S. Xiang, Z. Zhang, B. Chen, *Angew. Chem.* **2011**, *123*, 10696; *Angew. Chem. Int. Ed.* **2011**, *50*, 10510; g) J. An, C. M. Shade, D. A. Chengelis-Czegan, S. Petoud, N. L. Rosi, *J. Am. Chem. Soc.* **2011**, *133*, 1220; h) H. Furukawa, N. Ko, Y. B. Go, N. Aratani, S. B. Choi, E. Choi, A. Ö. Yazaydın, R. Q. Snurr, M. O'Keeffe, J. Kim, O. M. Yaghi, *Science* **2010**, *329*, 424; i) P. Dechambenoit, J. R. Long, *Chem. Rev. Soc.* **2011**, *40*, 3249; j) Y. Ling, Z. X. Chen, F. P. Zhai, Y. M. Zhou, L. H. Weng, D. Y. Zhao, *Chem. Commun.* **2011**, *47*, 7197.

[2] a) W. Lin, W. J. Rieter, K. M. L. Taylor, *Angew. Chem.* **2009**, *121*, 660; *Angew. Chem. Int. Ed.* **2009**, *48*, 650; b) W. J. Rieter, K. M. L. Taylor, H. An, W. Lin, W. Lin, *J. Am. Chem. Soc.* **2006**, *128*, 9024; c) A. M. Spokoyny, D. Kim, A. Sumrein, C. A. Mirkin, *Chem. Soc. Rev.* **2009**, *38*, 1218; d) Y. S. Li, H. Bux, A. Feldhoff, G. L. Li, W. S. Yang, J. Caro, *Adv. Mater.* **2010**, *22*, 3322; e) M. Jahan, Q. Bao, J. X. Yang, K. P. Loh, *J. Am. Chem. Soc.* **2010**, *132*, 14487; f) Y. Zhao, J. Zhang, B. Han, J. Song, J. Li, Q. Wang, *Angew. Chem.* **2011**, *123*, 662; *Angew. Chem. Int. Ed.* **2011**, *50*, 636; g) J. Puigmartí-Luis, M. Rubio-Martínez, U. Hartfelder, I. Imaz, D. Maspoch, P. S. Dittrich, *J. Am. Chem. Soc.* **2011**, *133*, 4216; h) W. Cho, S. Park, M. Oh, *Chem. Commun.* **2011**, *47*, 4138; i) A. Facchetti, *Angew. Chem.* **2011**, *123*, 6125; *Angew. Chem. Int. Ed.* **2011**, *50*, 6001.

[3] a) D. Tanaka, A. Henke, K. Albrecht, M. Moeller, K. Nakagawa, S. Kitagawa, J. Groll, *Nat. Chem.* **2010**, *2*, 410; b) T. Tsuruoka, S. Furukawa, Y. Takashima, K. Yoshida, S. Isoda, S. Kitagawa, *Angew. Chem.* **2009**, *121*, 4833; *Angew. Chem. Int. Ed.* **2009**, *48*, 4739; c) J. Cravillon, R. Nayuk, S. Springer, A. Feldhoff, K. Huber, M. Wiebcke, *Chem. Mater.* **2011**, *23*, 2130; d) H. Uehara, S. Diring, S. Furukawa, Z. Kalay, M. Tsotsalas, M. Nakahama, K. Hirai, M. Kondo, O. Sakata, S. Kitagawa, *J. Am. Chem. Soc.* **2011**, *133*, 11932; e) A. Umemura, S. Diring, S. Furukawa, H. Uehara, T. Tsuruoka, S. Kitagawa, *J. Am. Chem. Soc.* **2011**, *133*, 15506.

[4] a) L. E. Kreno, J. T. Hupp, R. P. V. Duyne, *Anal. Chem.* **2010**, *82*, 8042; b) G. Lu, O. K. Farha, L. E. Kreno, P. M. Schoenecker, K. S. Walton, R. P. V. Duyne, J. T. Hupp, *Adv. Mater.* **2011**, *23*, 4449.

[5] a) K. S. Novoselov, A. K. Geim, S. V. Morozov, D. Jiang, Y. Zhang, S. V. Dubonos, I. V. Grigorieva, A. A. Firsov, *Science* **2004**, *306*, 666; b) Y. Zhang, Y. W. Tan, H. L. Stormer, P. Kim, *Nature* **2005**, *438*, 201; c) J. W. Seo, Y. W. Jun, S. W. Park, H. Nah, T. Moon, B. Park, J. G. Kim, Y. J. Kim, J. Cheon, *Angew. Chem.* **2007**, *119*, 8984; *Angew. Chem. Int. Ed.* **2007**, *46*, 8828; d) J. S. Chen, X. W. Lou, *Electrochem. Commun.* **2009**, *11*, 2332; e) T. Sasaki, *J. Ceram. Soc. Jpn.* **2007**, *115*, 9; f) E. Yoo, J. Kim, E. Hosono, H. S. Zhou, T. Kudo, I. Honma, *Nano Lett.* **2008**, *8*, 2277; g) M. Osada, T. Sasaki, *J. Mater. Chem.* **2009**, *19*, 2503; h) K. Na, M. Choi, W. Park, Y. Sakamoto, O. Terasaki, R. Ryoo, *J. Am. Chem. Soc.* **2010**, *132*, 4169; i) S. Ida, C. Ogata, M. Eguchi, W. J. Youngblood, T. E. Mallouk, Y. Matsumoto, *J. Am. Chem. Soc.* **2008**, *130*, 7052; j) K. Maeda, M. Eguchi, S. H. A. Lee, W. J. Youngblood, H. Hata, T. E. Mallouk, *J. Phys. Chem. C* **2009**, *113*, 7962.

[6] a) S. Motoyama, R. Makiura, O. Sakata, H. Kitagawa, *J. Am. Chem. Soc.* **2011**, *133*, 5640; b) P. Z. Li, Y. Maeda, Q. Xu, *Chem. Commun.* **2011**, *47*, 8436; c) J. C. Tan, P. J. Saines, E. G. Bithell, A. K. Cheetham, *ACS Nano* **2012**, *6*, 615; d) S. Tricard, C. Costa-Coquelard, F. Volatron, B. Fleury, V. Huc, P. A. Albouy, C. David, F. Miserque, P. Jegou, S. Palacin, T. Mallah, *Dalton Trans.* **2012**, *41*, 1582; e) T. Bauer, Z. Zheng, A. Renn, R. Enning, A. Stemmer, J. Sakamoto, A. D. Schlüter, *Angew. Chem.* **2011**, *123*, 8025; *Angew. Chem. Int. Ed.* **2011**, *50*, 7879; f) P. Amo-Ochoa, L. Welte, R. González-Prieto, P. J. S. Miguel, C. J. Gómez-García, E. Mateo-Martí, S. Delgado, J. Gómez-Herrero, F. Zamora, *Chem. Commun.* **2010**, *46*, 3262.

[7] a) R. Lu, Y. Chen, H. Zhou, A. Yuan, *Acta Chim. Sin.* **2010**, *68*, 1199; b) E. Ruiz, S. Alvarez, R. Hoffmann, J. Bernstein, *J. Am. Chem. Soc.* **1994**, *116*, 8207; c) Y. Mathey, C. Mazieres, *Can. J. Chem.* **1974**, *52*, 3637; d) L. R. Falvello, M. Tomás, *Chem. Commun.* **1999**, 273.

[8] N. C. Li, A. Lindenbaum, J. M. White, *J. Inorg. Nucl. Chem.* **1959**, *12*, 122.

[9] K. E. Schwarzhans, *Angew. Chem.* **1970**, *82*, 975; *Angew. Chem. Int. Ed. Engl.* **1970**, *9*, 946.

[10] a) B. Liu, H. Shioyama, T. Akita, Q. Xu, *J. Am. Chem. Soc.* **2008**, *130*, 5390; b) D. Yuan, J. Chen, S. Tan, N. Xia, Y. Liu, *Electrochem. Commun.* **2009**, *11*, 1191; c) B. Liu, H. Shioyama, H. L. Jiang, X. B. Zhang, Q. Xu, *Carbon* **2010**, *48*, 456; d) J. Hu, H. Wang, Q. Gao, H. Guo, *Carbon* **2010**, *48*, 3599; e) B. Liu, X. Zhang, H. Shioyama, T. Mukai, T. Sakai, Q. Xu, *J. Power Sources* **2010**, *195*, 857; f) L. Radhakrishnan, J. Reboul, S. Furukawa, P. Srinivasu, S. Kitagawa, Y. Yamauchi, *Chem. Mater.* **2011**, *23*, 1225; g) H. L. Jiang, B. Liu, Y. Q. Lan, K. Kuratani, T. Akita, H. Shioyama, F. Zong, Q. Xu, *J. Am. Chem. Soc.* **2011**, *133*, 11854; h) M. Hu, J. Reboul, S. Furukawa, N. L. Torad, Q. Ji, P. Srinivasu, K. Ariga, S. Kitagawa, Y. Yamauchi, *J. Am. Chem. Soc.* **2012**, *134*, 2864.

[11] a) B. Liu, S. Han, K. Tanaka, H. Shioyama, Q. Xu, *Bull. Chem. Soc. Jpn.* **2009**, *82*, 1052; b) M. Hu, J. S. Jiang, Y. Zeng, *Chem. Commun.* **2010**, *46*, 1133; c) P. Durand, G. Fornasieri, C. Baumier, P. Beaunier, D. Durand, E. Rivière, A. Bleuzen, *J. Mater. Chem.* **2010**, *20*, 9348; d) X. Roy, J. K. H. Hui, M. Rabnawaz, G. Liu, M. J. MacLachlan, *Angew. Chem.* **2011**, *123*, 1635; *Angew. Chem. Int. Ed.* **2011**, *50*, 1597.

[12] a) K. C. Liu, M. A. Anderson, *J. Electrochem. Soc.* **1996**, *143*, 124; b) C. Yu, L. Zhang, J. Shi, J. Zhao, J. Gao, D. Yan, *Adv. Funct. Mater.* **2008**, *18*, 1544.

[13] a) B. Tian, X. Liu, H. Yang, S. Xie, C. Yu, B. Tu, D. Zhao, *Adv. Mater.* **2003**, *15*, 1370; b) F. Jiao, A. H. Hill, A. Harrison, A. Berko, A. V. Chadwick, P. G. Bruce, *J. Am. Chem. Soc.* **2008**, *130*, 5262; c) H. Liu, G. Wang, J. Liu, S. Qiao, H. Ahn, *J. Mater. Chem.* **2011**, *21*, 3046.

[14] R. R. Salunkhe, K. Jang, S. Lee, H. Ahn, *RSC Adv.* **2012**, *2*, 3190.

[15] a) C. C. Hu, K. H. Chang, T. Y. Hsu, *J. Electrochem. Soc.* **2008**, *155*, F196; b) C. Z. Yuan, X. G. Zhang, L. H. Su, B. Gao, L. F. Shen, *J. Mater. Chem.* **2009**, *19*, 5772.

